Characterization of GPS Clock and Ephemeris Errors to Support ARAIM

Todd Walter and Juan Blanch
Stanford University

ABSTRACT

GPS is widely used in aviation for lateral navigation via receiver autonomous integrity monitoring (RAIM). New methodologies are currently being investigated to create an advanced form of RAIM, called ARAIM that would also be capable of supporting vertical navigation. The vertical operations being targeted have tighter integrity requirements than those supported by RAIM. Consequently, more stringent evaluations of GNSS performance are required to demonstrate the safety of ARAIM.

ARAIM considers the possibility of two classes of satellite fault: those that affect each satellite independently and those that can affect multiple satellites simultaneously. These faults can lead to different safety comparisons in the aircraft. The likelihood of each fault type occurring can have a significant impact on the resulting ARAIM performance. Therefore, it is important to distinguish between such fault types and to determine appropriate models of their behavior and likelihood.

This paper examines the last seven years of GPS clock and ephemeris errors to determine appropriate estimates for the probability of independent satellite failures, P_{sat}, and the probability of simultaneous satellite failures P_{const}. Even more importantly, it evaluates performance when there are no failures present. Nominal signal accuracy is characterized by a conservative one-sigma parameter called user range accuracy (URA). This paper examines how well the true error distribution for each satellite is individually described by the broadcast URA value. It further examines how the errors across all satellites are correlated and could combine to create user-positioning errors.

INTRODUCTION

RAIM and ARAIM require a known minimum level of performance from the core constellations. Specifically, the nominal satellite ranging accuracy must be sufficiently characterized. Further, the likelihood that one or more satellites are in a faulted state (i.e. not in the nominal mode) must be conservatively described. The nominal performance is typically characterized as a Gaussian distribution with assumed maximum values for mean and sigma values. This modeled Gaussian distribution is an overbound of the true distribution [1] [2] (out to some probability level). The model also assumes that below some small probability, the likelihood of large errors can be much larger than would be expected according to the Gaussian distribution. This small probability corresponds to the combined fault likelihood.

The assumed performance level must be compatible with observed historical performance. Historical data can be used to set lower bounds for nominal accuracy and likelihood of faults. It is therefore important to carefully monitor satellite performance to determine the observed distribution of errors. This paper examines seven years of GPS data to in order to determine the distribution of ranging errors for each satellite.

SATELLITE ERROR SOURCES

The following threats [3] [4] are created by imperfections on board the satellites or at the constellation ground control centers:

- Satellite clock and ephemeris errors
- Ranging signal deformation errors
- Incoherence between the signal code and carrier
- Biases between signals at different frequencies
- Biases in the satellite's broadcast antenna

There are other error sources, such as those arising from the signal propagation environment or in the local aircraft environment. However, these other sources are cannot by controlled by satellite performance. They are dominated by ionospheric error, tropospheric error, multipath, and receiver antenna biases. For dual frequency ARAIM the ionosphere is directly estimated and the corresponding uncertainty is reduced.

The listed satellite threats contribute to nominal ranging errors, that is, the RF signals and navigation data are not perfect; there is some expected amount of error that is virtually always present. For GPS, this nominal error is bounded by the user range accuracy parameter σ_{URA}. In addition to the nominal errors, there is a small probability that faults lead to larger errors on one or more of the satellites. These rare faults are referred to as "narrow" if only one satellite may be affected and "wide" if more than one satellite may be affected. These faults are accounted for in the airborne algorithm and their likelihood of being present is specified by the parameters P_{sat} and P_{const}, respectively [5].

GPS SERVICE HISTORY

The largest errors in the above threat list normally are the clock and ephemeris errors. These errors have been characterized for GPS using data from the International GNSS Service (IGS) network [6]. The IGS network records the broadcast navigation data, in addition to the ranging measurements. The navigation data files are screened for outliers [7] and are then used to determine the real-time broadcast estimates for the satellite position and clock. Ranging measurements are used to create very precise, post-processed estimates of the satellite's position and clock over time. For this paper we used precise estimates provided by the National Geospatial-Intelligence Agency (NGA) [8]. These two estimates are differenced and the residual errors are projected along lines of sight to users on Earth. The navigation data also contains the σ_{URA}, which is used to normalize the residuals. These normalized residuals have been analyzed every fifteen minutes from January 1, 2008 through December 31, 2014.

Figure 1 shows an overview of the data analyzed. The vertical axis identifies each satellite observed by their service vehicle number (SVN). The colored squares on either side of the line indicate the colors that will be used to plot individual satellite data in subsequent plots. Each horizontal line indicates a type of measurement for each satellite. Green indicates that the broadcast ephemeris was set healthy and a valid comparison to the precise ephemeris was obtained (the data set contains 7,406,653 such comparisons). Blue indicates that the broadcast ephemeris was set to unhealthy and therefore no comparison was made. Magenta indicates that no broadcast ephemeris was obtained from the IGS database, but that there were precise orbit data. Yellow indicates that broadcast ephemerides were obtained, but no precise orbit data was available. Finally black indicates that the

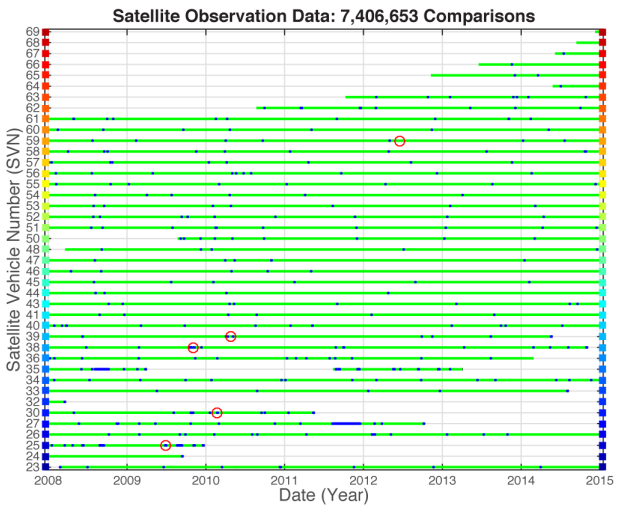

Figure 1. *Summary of observations for each satellite, where green indicates good observations, blue that the satellite is unhealthy, and red circles indicate a fault*

satellite was operational, but we have neither broadcast or precise orbit data. The gray background line indicates that the satellite was not operational (e.g. not yet launched, decommissioned, or not broadcasting).

There are no magenta, yellow, or black points in this figure because when such points are first identified, we determine the cause and attempt to fill in any missing data. In most cases, the data loss is because the satellite is not broadcasting a usable signal. These situations are not readily apparent in either the broadcast or precise data files. However, by examining the observation files we can see that the vast majority of receivers are not tracking the signal. In one instance, we were able to replace missing NGA data with precise IGS clock estimates. Thus, we are certain that for this time period we have valid broadcast and precise ephemerides for every fifteen-minute period that a GPS satellite was transmitting a healthy, usable signal.

According to the GPS standard positioning service performance standard (GPS SPS PS) [9] a satellite is considered to have a major service failure if the average projected error is greater than 4.42 x σ_{URA}. We use a stricter criterion in our evaluation. We declare a satellite to be faulted if the projected error at any point on the earth is greater than 4.42 x σ_{URA}. This difference is important because we are concerned with the performance of all satellites and wish to protect the most vulnerable user and not merely the average of all users.

Red circles in Figure 1 indicate times when the maximum projected error (MPE) exceeds 4.42 x σ_{URA}. There are five such events with about 1.75 cumulative satellite

hours in a faulted state over this seven-year period. These events correspond to:

PRN	SVN	Date	UTC Time
25	25	June 26, 2009	09:05 – 09:45
8	38	November 5, 2009	18:45 – 19:02
30	30	February 22, 2010	20:45 – 20:52
9	39	April 25, 2010	19:40 – 19:55
19	59	June 17, 2012	00:10 – 00:36

Each event has been studied in greater detail by combining the fifteen-minute NGA precise clock and ephemeris data with five-second precise clock data from the center for orbit determination in Europe (CODE) [10]. The NGA orbits are interpolated to a five second rate and the CODE clocks are adjusted to match the NGA clocks at the fifteen-minute intervals.

Figure 2 shows the June 26, 2009 event affecting PRN 25. As can be seen in the second panel, at 09:05 the clock jumped by about 20 m. The orbit was not affected by this transition. The broadcast URA was 2.4 m throughout. The third panel shows the issue of data: clock (IODC) for the corresponding broadcast ephemeris. IODC 12 was in affect indicating the satellite was healthy and had a URA of 2.4 m. The bottom panel shows the signal to noise ratio (SNR) for all 156 IGS stations that were tracking the satellite at this time [11]. After 09:45:00 all but eight stations stop reporting data for the satellite, after 09:45:30 seven of the eight remaining station stations stop reporting data. It appears that just after 09:45:00 something about the satellite signal changed to make it difficult to track. Note that the lone station that claims to track the satellite at this time only started tracking it 09:44:30 and shows pseudorange discontinuities when normal tracking resumes after 10:23.

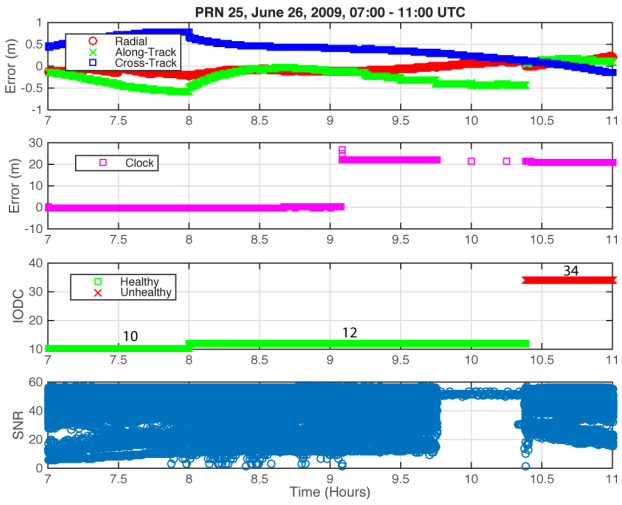

Figure 2. *Fault event for PRN 25 on June 26, 2009*

GPS satellites have several methods to indicate that the satellite is unhealthy. Primarily there is a health bit in the broadcast ephemeris message. However, this is only broadcast every 30 seconds. It can take an even longer time to generate and upload new ephemeris content. GPS can more quickly indicate faults by switching to either non-standard code (NSC) or default data [12] [13]. NSC is simply having the satellite switch to another PRN code, one that the user is not expecting (and isn't being broadcast by another satellite). Default data is a series of alternating ones and zeros that will fail to pass parity when the user seeks to decode the navigation data.

The use of NSC is not ideal as the user can still unintentionally track a cross-correlation peak. Such cross-correlation tracking should have a 24 dB-Hz lower SNR [14]. Thus, a high elevation satellite is more likely to be accidently tracked in this mode than a low elevation satellite. Receivers should employ screening to prevent use of satellites whose power level is more than ~ 20 dB-Hz lower than expected.

Default data will cause parity to consistently fail and aviation receivers will not use a satellite after consecutive parity faults. The use of NSC is the primary method to quickly prevent GPS faults from affecting users. Eventually, the satellite needs to return to its assigned PRN code and start broadcasting data either with the health bit set to "unhealthy" or with data that corrects the problem. As can be seen in Figure 2. This occurs around 10:23 when new ephemeris data is received with IODC = 34 and indicating an unhealthy status. An aviation user must take care when the signal first comes back after such a fault. The IODC = 12 data is still within its valid time period and it could take 30 or more seconds to receive the unhealthy indication. An aviation receiver should not immediately use a satellite that it has not seen for more than ten minutes until the receiver has revalidated the broadcast ephemeris.

Notice that in the second panel of Figure 2 that the NGA clock still has solutions at fifteen-minute intervals during the outage while the CODE five-second solution does not exist during this outage period. This may indicate that the NGA data is able to track the satellite on its alternate PRN. It is also possible that this data is merely extrapolated or interpolated from the surrounding periods when the normal PRN code and data are broadcast.

Figure 3 shows the November 5, 2009 event affecting PRN 8. Instead of a sudden clock jump as was seen before, this event appears to be a clock ramp. Again the orbital position is not affected. The ramp appears to begin around 18:15 and continue until 19:02 when all

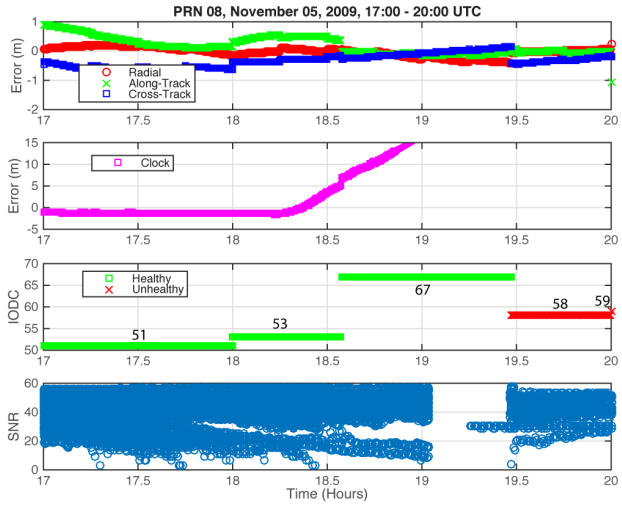

Figure 3. *Fault event for PRN 8 on November 5, 2009*

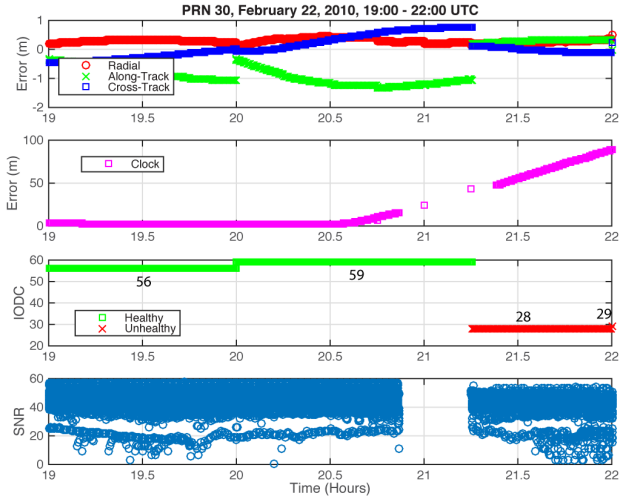

Figure 4. *Fault event for PRN 30 on February 22, 2010*

tracking stops. For this event there were 135 IGS stations tracking the satellite. Eventually two of them start tracking again during the apparent outage, but with SNRs reduced by about 24 dB-Hz. Thus, these two appear to be tracking a cross-correlation peak. The remaining stations do not resume tracking until 19:28. The broadcast URA was 2.4 m throughout.

The ramp begins while IODC = 53. Part way through a new ephemeris is broadcast with IODC = 67. This causes a discontinuity in the observed clock error, but does not correct the clock drift. The error becomes larger than 4.42 x σ_{URA} at about 18:44:45, and remains so until 19:02 when the satellite becomes untrackable. At around 19:28, regular transmission resumes with a new ephemeris set with IODC = 58 indicating that the satellite is unhealthy.

Figure 4 shows the February 22, 2010 event affecting PRN 30. This event is another clock ramp very similar to the previous fault. The apparent ramp starts shortly after 20:30 and creates an error larger than 4.42 x σ_{URA} at about 20:45:30. After 20:51:30 all but ten of the 108 IGS stations tracking the satellite stopped reporting data and those ten all stopped after 20:52:00. Tracking starting again at 21:15:00 and new ephemeris data with IODC = 28 was received indicating that the satellite was unhealthy. This new ephemeris also corrected the larger than normal ephemeris errors but did not correct the clock drift. Also the NGA clock data exists during the outage, but the precise CODE clock data does not. The broadcast URA was 2.4 m throughout.

Figure 5 shows the April 25, 2010 event affecting PRN 9. This fault is noticeably different from the three prior events. The top two panels clearly show that now the fault is in the orbital information and is almost exclusively in the cross-track component. At about 19:26:00, the broadcast ephemeris information changes

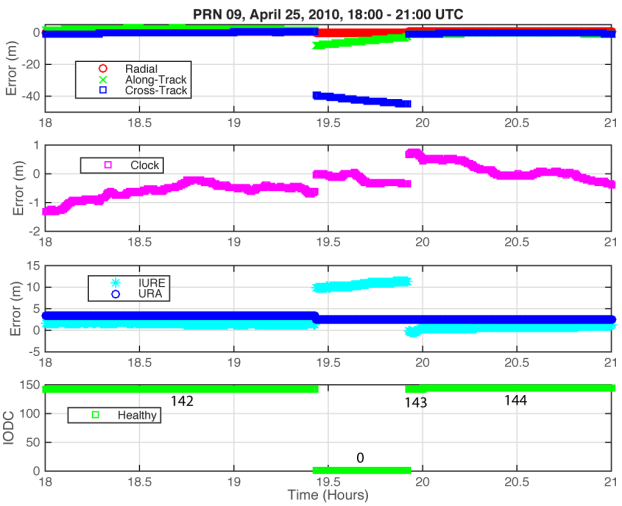

Figure 5. *Fault event for PRN 9 on April 25, 2010*

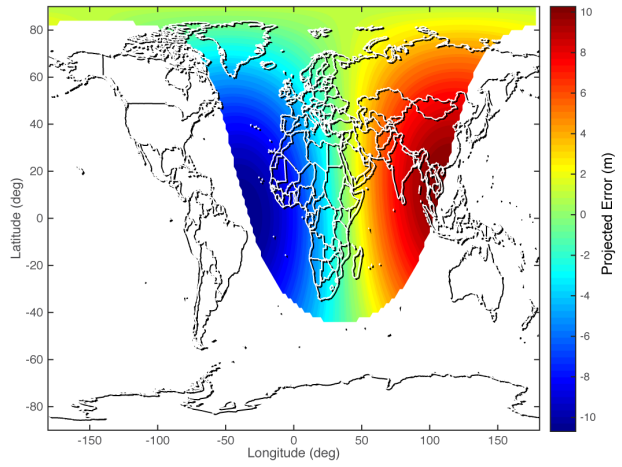

Figure 6. *Projected error for April 25, 2010 event*

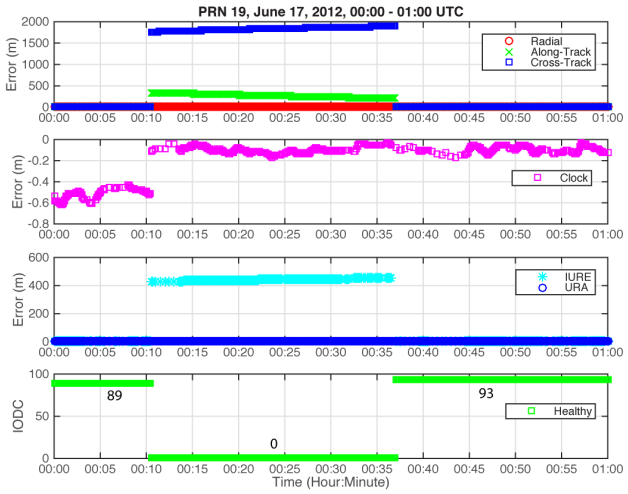

Figure 7. *Fault event for PRN 19 on June 17, 2012*

from the data with IODC = 142 to the data set with IODC = 0. This new set reduces the clock error slightly, but introduces a 40 m cross-track error. It also lowered the URA from 3.4 m to 2.4 m. The third panel shows that the MPE is just about 10 m. Because the URA is now the minimum value of 2.4 m a fault will be declared if the MPE exceeds 10.6 m, which occurs around 19:40:30. The fault is corrected at 19:55:30 when new ephemeris data with IODC = 143 is broadcast.

Note that this fault is not considered a major service failure because the official definition calculates the error averaged over the surface of the earth. In our calculation, the MPE barely exceed 4.42 x σ_{URA}, the average value is several meters below. Figure 6 shows a map of the projected error near the peak of the fault. The cross-track error is maximized for users in Southeast Asia and in the Atlantic Ocean, but user in Europe will not see as large an error. We will consider this event a fault and count it against P_{sat}, even though officially this event does not qualify as a major service failure.

Figure 7 shows the June 17, 2012 event affecting PRN 19. This event is very similar to the prior fault. Again the fault is predominantly in the cross-track direction, although now there is a sizeable along-track error as well. However, this fault is sufficiently large that there is no debate as to whether or not to label it a major service failure. At about 00:10:30, the broadcast ephemeris information changes from the data with IODC = 89 to a data set with IODC = 0. This new set reduces the clock error, but introduces a 1700 m cross-track error. The URA remains at 2.4 m throughout. The MPE is over 400 m. The fault is corrected at 00:37:00 when new ephemeris data with IODC = 93 is broadcast.

OBSERVED GPS FAULT PROBABILITIES

The next sections describe the nominal behaviors arising from the previously listed threats. The prior section showed that these threats can lead to rare faults that are not well described by the nominal parameters. The next section will make it is obvious that, on average, errors below 4.42 x σ_{URA} occur no more frequently than would be expected from a Gaussian distribution. Faults, however, require separate handling. ARAIM airborne algorithms [5] compare subset solutions to find inconsistencies. As long as the true probability of encountering such failures is below the assumed probability, the airborne algorithm can maintain integrity as expected. The GPS SPS PS states that there will be no more than 10^{-5} probability of satellite fault, per satellite, per hour. The commitment further states that major service failures will be flagged or removed within six hours. A satellite fault observed at any given time could have initiated sometime in the prior six hours and now be present to affect the user. These specifications imply an extreme upper bound for the probability that any given satellite observation is faulty, P_{sat}, of 6 x 10^{-5}.

Figure 1 shows the history of GPS satellite observation from January 2008 through December 31, 2014. In that time, there have been five faults observed with a cumulative duration of just over 1.75 hours. The collected data consisted of more than 1.8 million valid satellite hours, where the satellites were broadcasting valid signals and indicating that they were healthy. The observed data implies an average onset fault rate of ~2.7 x 10^{-6}/hour/satellite, an average fault duration of ~21 minutes and an average value for P_{sat} of approximately 9.5 x 10^{-7}. Thus, there is more than a factor of 60 between the observed fault probability and the extreme upper bound from the commitment. The numbers in the GPS SPS PS (10^{-5} probability of fault onset/satellite/hour and six hours to alert) are meant to represent upper bounds, not expected values. The product of two upper bounds creates an even more conservative value. Traditional RAIM assumes a 10^{-4}/hour probability that one of the satellites in view may have a failure [15]. By assuming that there are ten satellites in view (and a one hour fault duration) this corresponds to a value of 1 x 10^{-5} for P_{sat}. This value, while smaller than the extreme upper limit of the commitment is still at least ten times greater than the historically observed value. It represents a good compromise and is a value that we endorse for use in describing P_{sat} for GPS for ARAIM.

In addition to narrow faults, there is concern over the possibility of wide faults or faults that can lead to

uncharacteristically large errors on more than one satellite at a time. The GPS performance commitment does not prohibit the possibility that the faults occur concurrently. The upper limit of 10^{-5} faults per satellite per hour implies approximately three satellite faults within any given year for a constellation of ~30 satellites. Again using a six-hour upper bound and assuming at least two of these faults occur concurrently would imply an upper limit for P_{const} of approximately 7 x 10^{-4}. No concurrent major service failures have ever been observed on healthy GPS satellites since it was declared operational in 1995. However, over the ensuing twenty year time frame, it would be difficult to empirically demonstrate values below ~5 x 10^{-6}. Furthermore, it is not clear whether operations from more than ten years ago are as relevant to current operation. Our seven-year data span corresponds to a little more than 61,000 constellation hours. Therefore, an empirical upper bound of order 10^{-5} appears to be reasonable. We have found that it makes little difference in performance whether we use 10^{-4} or 10^{-5} [3], so we have initially proposed using 10^{-4} to be conservative. At first glance, it appears contradictory to use a value for P_{const} that is equal to or greater than P_{sat}. However, the numbers are describing different types of events and are not directly comparable. Because there are ~30 GPS satellites but only one GPS constellation, using the same probability for P_{sat} and P_{const} means that the likelihood of a narrow satellite failure being present is still 30 time more likely than a wide failure being present at any given time.

NOMINAL RANGING ACCURACY

The GPS satellites broadcast σ_{URA} to indicate the expected level of accuracy. Figure 8 shows the relative frequency of the different broadcast values by satellite block and across the whole constellation. The most likely value by far is also the minimum currently available number of 2.4 m. This value is sent more than 92% of the time for the newest Block IIF satellites. The next most common value is 3.4 m. This value is typically used for older data that was uploaded to the satellite approaching 24 hours earlier. This larger value is sent more than 7% of the time for all blocks. Together these values account for nearly 99.85% of all σ_{URA}s broadcast for the Block IIF satellites. The older satellites are more likely to send out larger values. The larger values indicate the possibility of larger errors, but typical performance is not much worse when 3.4 m values are sent than when 2.4 m values are broadcast.

Figure 9 shows the observed probability density functions (PDFs) for the radial, along-track, cross-track, clock, and projected errors. The errors appear to be very well behaved to down to fairly low probability. The errors appear quasi-gaussian, but there is ample evidence of mixing around 10^{-3} and below. The overall mean value, 68% containment bound, and 95% bound are shown in the included table. Also listed is an overbounding sigma value, σ_{ob}, that was calculated excluding the worst 0.001% of the data (effectively bounding to a 10^{-5} level).

Figure 10 and Table 1 (at the end of the paper) describe these values for each individual satellite as well as grouped by block and for the aggregate total. The green bars show the 68% bound, the red bars indicate the σ_{ob} term, and the black lines indicate the mean value. It is obvious that the radial errors are the smallest and along-track errors are the largest. The projected instantaneous user range errors (IUREs) are most similar to the clock

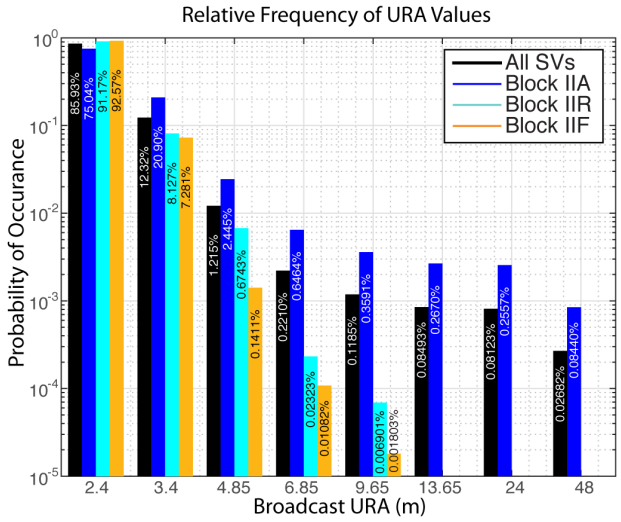

Figure 8. *Relative frequencies for broadcast σ_{URA} values.*

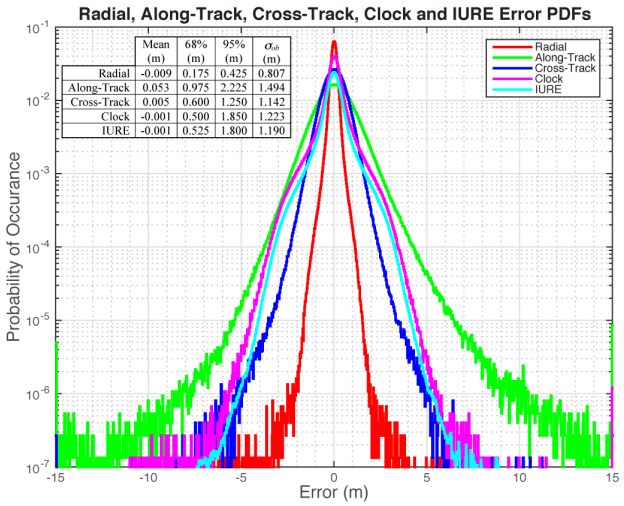

Figure 9. *Radial, along-track, cross-track, clock, and projected error distributions*

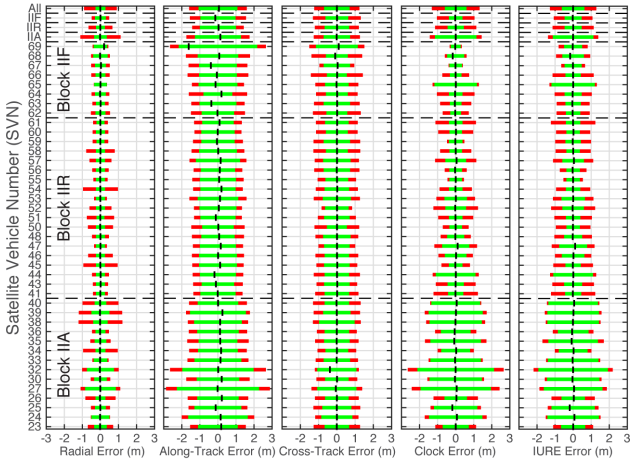

Figure 10. *Radial, along-track, cross-track, clock, and projected error values. The green bars show the 68% bound, the red bars indicate the σ_{ob} term, and the black lines indicate the mean value.*

errors. All but the oldest and the very newest satellite have similar along-track and cross-track performance. The Block IIA satellites have the worst clock performance, except for SVN 65 which is the only Block IIF using a cesium clock. Rubidium clocks exhibit better performance. SVN 69 is the only satellite with a noticeable bias. However, this satellite only entered into service late on December 12, 2014 and therefore only includes about eighteen operational days of data. Table 1 at the end of the paper also includes specific values and the 95% containment bounds.

OBSERVED ERROR DISTRIBUTION

The observed failures provide an indication of the historical fault rate. Although it is possible that faults create errors smaller than 4.42 x σ_{URA}, typically observed faults quickly grow to much larger errors or are quickly removed from effect. Similarly, nominal Gaussian performance would be expected to occasionally create errors greater than 4.42 x σ_{URA}. However, we have not seen any evidence of this behavior. As we will show, in almost all cases, the errors are well below the major service failure threshold, and when they are above it, they are most often well above it.

One minus the cumulative distribution function (CDF) of the MPE for each individual satellite is shown in Figure 11 and CDFs grouped together by GPS satellite block type are shown in Figure 12. The heavy black line in both plots shows the aggregate CDF incorporating all satellites. The rightmost red line shows the expected CDF value corresponding to a normal distribution with a zero-mean and unity variance. This red line is only extended down to the 10^{-5} probability level, since this is the specified satellite fault rate in the GPS SPS PS. We do not require nominal Gaussian behavior below this line.

Only two of the observed faults were large enough and lasted long enough, compared to the total amount of data for the satellite, to affect the CDF above the 10^{-5} level (SVNs 25 & 30). Two other faults are just barely below the 10^{-5} level (SVNs 38 & 59). The fault on SVN 39 was sufficiently short and small so as to have little visible impact on the CDF. Whether or not satellites fall above or below the 10^{-5} level is also largely dependent on the total amount of data for each satellite. Satellites with shorter histories will be more likely to appear bad in Figure 11.

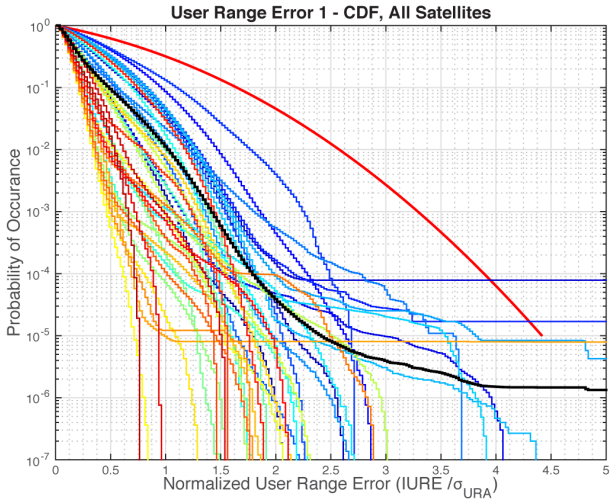

Figure 11. *CDF of normalized maximum projected ranging errors for all satellites.*

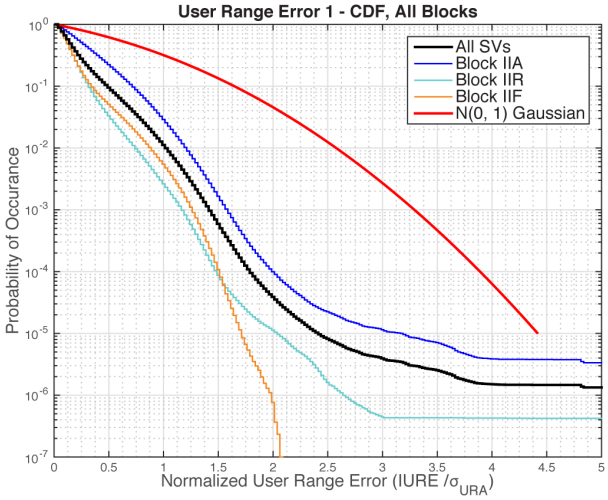

Figure 12. *CDF of normalized maximum projected ranging errors grouped by satellite block.*

Figure 12 shows what the distributions look like when combined for the various GPS satellite blocks. Combining data together by blocks is a better method to evaluate the satellite fault probabilities. The five individual satellites that experienced faults were probably no more likely to do so than the other members of their respective blocks. However, the designs of the satellites are different form block to block, so it is reasonable to expect differences in fault probabilities. It appears that performance has improved over time and that the oldest, Block IIA, have the largest errors and fault likelihood. The newest, Block IIF have yet to experience any faults (in fact, no errors larger than 2.1 x σ_{URA} have been observed for this block). For all three blocks, the nominal clock and ephemeris errors are very conservatively described by the broadcast σ_{URA} value down to well below the 10^{-5} level. The broadcast σ_{URA} would still be safe if it were significantly reduced. Additional partitioning of the data will be performed to further look for satellite specific effects or short-term effects [16] [17].

Figures 11 and 12 indicate that there is quite a bit of margin between the theoretical Gaussian CDF (heavy red line) and the actual CDFs. It is possible to calculate the minimum scale factor, that when multiplied by the broadcast σ_{URA}, causes the CDF to just touch the red line, but otherwise remain below it. This scale factor is the ratio of the minimum overbounding sigma to the broadcast σ_{URA}. We determined this ratio using only data when the broadcast σ_{URA} was 2.4 m and then multiplied it by the 2.4 m value to determine the minimum average overbounding σ_{URA}. Figure 13 plots these values for each satellite. As is evident from the figure, most of these ratios were below 0.5, leading to minimum σ_{URA} values below 1.2 m, especially for the later Block IIR and IIF satellites. In fact the average is well under a meter. This is significant because future messages from GPS will be able to broadcast smaller values of σ_{URA}. Figure 13 indicates the smaller values and the fact that most Block IIR and IIF satellites would be able to transmit values below 0.85 m.

NOMINAL GPS POSITIONING ACCURACY

Although the individual satellite error distributions may be Gaussian bounded to the desired level, it is even more important to quantify how these satellite errors combine together to create the position error. If the satellite errors are correlated, they can combine to form unexpectedly large position errors. The protection level equations bound the position errors by treating the satellite errors as though they are independent from one another. It is

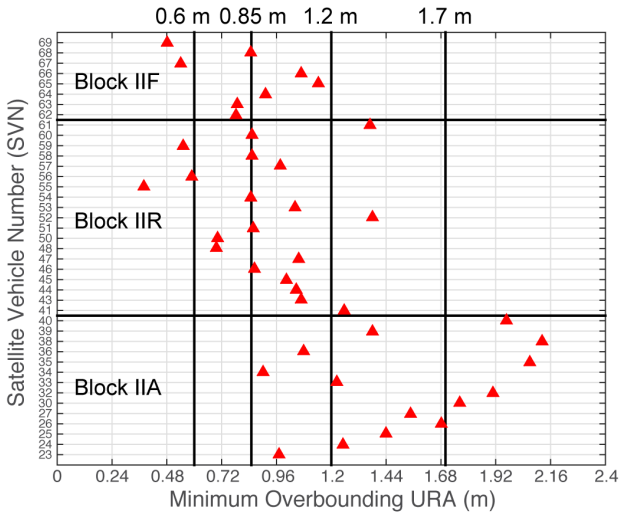

Figure 13. *Ratio of the minimum bounding sigma to the broadcast σ_{URA}.*

essential to determine whether or not this approach is correct. At each time step and user location, a weighted common-mode error is subtracted from each projected satellite error at that location. This residual is then divided by its corresponding σ_{URA}. All of the residuals are then squared, summed together, and a square root of the whole is taken. This process was repeated at 200 evenly spaced user locations and for the 245,472 15-minute time steps in this period. If all of the errors at a specific location are large at the same time, this chi-square value will be large.

Figure 14 shows the probability density function of this square root of the sum of the squared normalized errors (after removing satellites with major service failures) and Figure 15 shows one minus the CDF of the same. This metric evaluates the behavior of unfaulted subset solutions [5]. The protection level is a valid overbound of the position error if at least one subset contains only unfaulted measurements and the corresponding position error is conservatively characterized.

The histograms in Figures 14 and 15 demonstrate that the clock and ephemeris errors are exceedingly well behaved. At no time was there more than one faulty GPS satellite present in the constellation. Further, it is evident that when one satellite has a large value (e.g. > 2 x σ_{URA}) the other values must all be well below 1 x σ_{URA}. If all of the satellites simultaneously had errors even as large as 1 x σ_{URA}, the RSS value would correspond to the number of satellites in view. However, the largest observed value is just over four, while the average number in view is most commonly nine or ten.

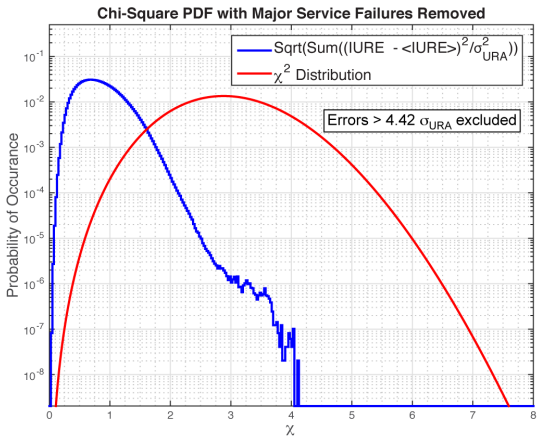

Figure 14. *PDF for chi-square of the normalized ranging errors.*

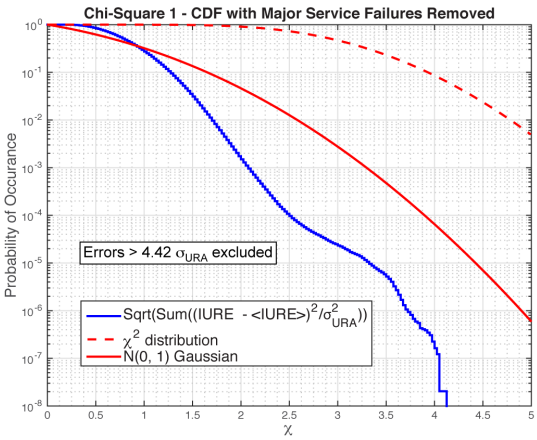

Figure 15. *CDF for chi-square of the normalized ranging errors.*

The RSS satellite errors show even greater reduction compared to the expected chi-square distribution than can be seen in the individual satellite error distributions compared to the Gaussian distribution in Figures 11 and 12. This indicates that the positioning errors of the unfaulted subsets will have significant margin against the formal error term used in the protection level equation [16] and that treating the errors as though they are independent is conservative. Figures 11 - 15 clearly demonstrate that the historically broadcast σ_{URA} values for GPS conservatively describe the observed clock and ephemeris error down to probabilities of 10^{-5} and lower.

GPS NOMINAL BIAS ERRORS

The other GPS error sources listed previously have very different characteristics and are described via other analyses. One such error source arises from subtle variations in the shape of the broadcast waveform from the satellite. Rather than containing perfectly rectangular chips, the signals have imperfections in their formation caused by subsequent filtering via various components of the transmission chain [18] [19]. Each satellite has slightly different imperfections than the others. This so called nominal deformation effect leads to small differences in ranging measurements made by different receivers to different satellites. The magnitude of the difference depends on user receiver characteristics. Studies have shown that for very different receiver designs, these biases can be on the order of one meter. However, by limiting the receiver design space and by increasing commonality with the reference receivers, these errors can be reduced to being on the order of 10 cm [20].

Another concern is the possibility of misalignment between the code and carrier portions of the ranging signals. If these are not in perfect coherence, the act of carrier smoothing will introduce a bias that increases with the length of the smoothing time. The code and carrier have never been observed to be incoherent on GPS L1 signals. However, such an effect has been observed on the L5 signals of the GPS Block IIF satellites. The magnitude of that error appears to be on the order of 10 cm [21][22]. However, for most satellites, the nominal effect is expected to be much smaller.

The iono-free combination of the L1 and L5 signals assumes that the two signals are synchronized in time at their broadcast. However, electronic components introduce different amounts of signal delay at different frequencies. Thus, the signals at two different frequencies have an offset that is nominally constant. The value of this inter-frequency bias is estimated and broadcast to the user as part of the navigation data. However, this inter-signal correction has some uncertainty, as the estimation process is affected by noise. This nominal effect of this error term is included in the satellite clock estimate error.

The final threat to be considered comes from the satellite antenna. Ideally each antenna is treated as a point source for the signals. However, real antennas have biases that vary with look angle. That is, the path length from the antenna appears to be different depending on the direction to the user. These biases affect code and carrier differently and are also different for the two frequencies. Great effort has been made to minimize the satellites' carrier phase antenna biases; they appear to be below 4 cm in variation. Unfortunately, the code phase variations have been observed up to 50 cm in variation [23].

The satellite ephemeris, clock, and inter-frequency bias nominal errors are stochastic and continuously changing. These other errors are nearly constant and can be viewed as closer to being deterministic. ARAIM therefore will treat them as a constant offset to the Gaussian overbound and use the term b_{nom} to bound the nominal errors arising from signal deformation, code-carrier incoherence, and antenna phase center variations. In reality, σ_{URA} and b_{nom} together must bound the convolution of all of the errors with sufficient probability. At the moment, both parameters are very conservatively calculated. The minimum possible GPS broadcast σ_{URA} value has a corresponding sigma of 2.4 m (lower values will become possible within the next few years). When smaller URA values are broadcast in the future, it will be necessary to again carefully scrutinize the behavior and it is possible that there will be reduced margin at that time. As described above, the three bias terms together nominally can be conservatively bounded by a 75 cm value for b_{nom} [24].

CONCLUSIONS

We have analyzed seven years of GPS data in order to characterize its nominal accuracy and the probabilities of having a satellite or more than one satellite in a faulted state. We have found that the broadcast σ_{URA} values very conservatively describe the clock and ephemeris errors. There is significant margin to broadcast even smaller values. We further have found that GPS significantly exceeds its commitment that would allow up to approximately three six-hour satellite faults per year. Instead we have found a total of five faults over seven years with cumulative fault duration of approximately 1.75 hours. This observation corresponds to a value of 9.5×10^{-7}, which is well below our recommended value for probability of a satellite being in a fault state, P_{sat}, of 10^{-5}. Each observed fault was studied and presented here in greater detail

We have not observed any instances of simultaneous faults on more than one satellite. Further, we are not aware of constellation wide faults that would affect a dual-frequency user occurring on GPS since it was declared fully operational in 1995. We have therefore recommended the very conservative value of 10^{-4} for P_{const}, primarily due to the limited number of constellation hours that have occurred in this period. This is a very difficult number to restrict empirically.

We also examined the correlation of the errors across multiple satellites in view at the same time. We found that the errors are not significantly correlated and that treating them as though they are independent is sufficiently conservative. We plan to continue to parse the data looking for smaller anomalies and other irregular behavior.

ACKNOWLEDGMENTS

The authors would like to gratefully acknowledge the FAA Satellite Product Team for supporting this work under Cooperative Agreement 2012-G-003. We also grateful to the U.S. - EU Working Group-C (WGC) ARAIM working group for the continues discussions on the potential implementation of ARAIM. The opinions expressed in this paper are the authors' and this paper does not represent a government or WGC position on the future development of ARAIM.

REFERENCES

[1] Walter, T., Rife, J., and Blanch, J., "Treatment of Biased Error Distributions in SBAS," *Proceedings of GNSS 2004*, Sydney, Australia, December 2004.

[2] DeCleene, B., "Defining Pseudorange Integrity - Overbounding," *Proceedings of the 13th International Technical Meeting of the Satellite Division of The Institute of Navigation (ION GPS 2000)*, Salt Lake City, UT, September 2000, pp. 1916-1924.

[3] Working Group C, ARAIM Technical Subgroup, Interim Report, Issue 1.0, December 19, 2012. Available at: http://ec.europa.eu/enterprise/newsroom/cf/_getdocument.cfm?doc_id=7793, or http://www.gps.gov/policy/cooperation/europe/2013/working-group-c/ARAIM-report-1.0.pdf

[4] Blanch, J., Walter, T., Enge, P., Wallner, S., Fernandez, F. A., Dellago, R., Ioannides, R., Hernandez, I. F., Belabbas, B., Spletter, A., and Rippl, M., "Critical Elements for a Multi-Constellation Advanced RAIM", *NAVIGATION, Journal of The Institute of Navigation*, Vol. 60, No. 1, Spring 2013, pp. 53-69.

[5] Blanch, J., Walter, T., Enge, P., Lee, Y., Pervan, B., Rippl, M., Spletter, A., "Advanced RAIM user Algorithm Description: Integrity Support Message Processing, Fault Detection, Exclusion, and Protection Level Calculation," *Proceedings of the 25th International Technical Meeting*

of The Satellite Division of the Institute of Navigation (ION GNSS 2012), Nashville, TN, September 2012.

[6] Dow, J.M., Neilan, R. E., and Rizos, C., "The International GNSS Service in a changing landscape of Global Navigation Satellite Systems," *Journal of Geodesy* (2009) 83:191–198, DOI: 10.1007/s00190-008-0300-3

[7] Heng, L., Gao, G. X., Walter, T., Enge, P., "GPS Signal-in-Space Anomalies in the Last Decade: Data Mining of 400,000,000 GPS Navigation Messages," *Proceedings of the 23rd International Technical Meeting of The Satellite Division of the Institute of Navigation (ION GNSS 2010*), Portland, OR, September 2010, pp. 3115-3122.

[8] http://earth-info.nga.mil/GandG/sathtml/ephemeris.html

[9] Global Positioning System Standard Position Service Performance Standard, 4th Edition, September 2008

[10] Bock, H., Dach, R., Jaggi, A., and Beutler, B., "High-rate GPS clock corrections from CODE: support of 1 Hz applications," J Geodesy, 2009, 83(11):1083–1094. doi:10.1007/s00190-009-0326-1

[11] http://www.igs.org/products/data

[12] Kovach, K. and Conley, R., "SATZAP: A Novel Approach to GPS Integrity", NAVIGATION, Journal of The Institute of Navigation, Vol. 38, No. 2, Summer 1991, pp. 163-190.

[13] Kovach, K., Berg, J., and Lin, V., "Investigation of Upload Anomalies Affecting IIR Satellites in October 2007" presented at Stanford University's PNT Challenges and Opportunities Symposium, November 2008. http://scpnt.stanford.edu/pnt/pnt2008.html

[14] Balaei, A. T. and Akos, D. M., "Cross Correlation Impacts and Observations in GNSS Receivers", NAVIGATION, Journal of The Institute of Navigation, Vol. 58, No. 4, Winter 2011-2012, pp. 323-333.

[15] Minimum Operational Performance Standards for Global Positioning System / Aircraft-Based Augmentation System Airborne Equipment, RTCA document DO-316, April 2009.

[16] Walter, T., Blanch, J., Enge, P., "Evaluation of Signal in Space Error Bounds to Support Aviation Integrity", *NAVIGATION, Journal of The Institute of Navigation*, Vol. 57, No. 2, Summer 2010, pp. 101-113.

[17] Global Positioning System (GPS) Standard Positioning Service (SPS) Performance Analysis Report available at http://www.nstb.tc.faa.gov/reports/PAN82_0713.pdf

[18] Phelts, R.E., Blanch, J., Walter, T., and Enge, P., "The Effect of Nominal Signal Deformation Biases on ARAIM Users," *Proceedings of the 2014 International Technical Meeting of The Institute of Navigation*, San Diego, California, January 2014, pp. 56-67.

[19] Phelts, R.E., Altshuler, E., Walter, T., and Enge, P., "Validating Nominal Bias Error Limits Using 4 years of WAAS Signal Quality Monitoring Data," in Proceedings of the ION Pacific PNT Meeting, Honolulu, HI, April 2015.

[20] Wong, G., "Impact of Nominal Signal Deformations on Satellite Navigation Systems," Stanford University Ph.D. Thesis, 2014

[21] Montenbruck, O., Hauschild, A., Steigenberger, P., and Langley, R. B., "Three's the Challenge," *GPS World*, July, 2010.

[22] Montenbruck, O., Hugentobler, U., Dach, R., Steigenberger, P., and Hauschild, A., "Apparent clock variations of the Block IIF-1 (SVN62) GPS satellite," GPS Solutions, Volume 16, Issue 3, July 2012, pp 303-313.

[23] Haines, B., Yoaz B.-S., Bertiger, W., Desai, S., and Weiss, J., "New GRACE-Based Estimates of the GPS Satellite Antenna Phase- and Group-Delay Variations," 2010 *International GNSS Service (IGS) Workshop*, Newcastle upon Tyne, England, 28 June to July 2010, ftp://stella.ncl.ac.uk/pub/IGSposters/Haines.pdf

[24] Macabiau, C., Milner, C., Tessier, Q., Mabilleau, M., Vuillaume, J., Suard, N., Rodriguez, C., "Impact of Nominal Bias Bounding Techniques on Final ARAIM User Performance," *Proceedings of the 2014 International Technical Meeting of The Institute of Navigation*, San Diego, California, January 2014, pp. 68-77.

		Radial				Along-Track				Cross-Track				Clock				IURE			
	SV	**mean**	**68%**	**95%**	**σ_{ob}**	**mean**	**68%**	**95%**	**σ_{ob}**	**mean**	**68%**	**95%**	**σ_{ob}**	**mean**	**68%**	**95%**	**σ_{ob}**	**mean**	**68%**	**95%**	**σ_{ob}**
Block IIA	**23**	-1.9	25	45	60	18.0	100	225	144	-0.1	58	128	117	0.0	63	133	103	0.0	58	133	101
	24	-2.1	40	70	43	14.5	155	315	191	0.6	75	165	109	6.8	138	268	162	6.8	133	263	142
	25	-0.7	20	43	43	-12.3	120	258	153	-0.6	70	143	119	-18.9	110	250	130	-18.9	110	253	131
	26	-2.6	18	38	74	21.2	105	245	157	0.4	55	120	110	3.8	53	123	113	3.8	55	130	110
	27	-0.7	75	120	100	-2.2	218	423	278	-5.8	98	205	129	5.1	185	338	233	5.1	153	293	177
	30	-1.9	25	50	45	20.6	108	250	166	1.2	55	123	102	-3.9	135	263	147	-3.9	135	265	147
	32	-3.0	65	103	91	1.4	188	343	256	-37.6	98	180	111	-0.4	203	373	256	-0.4	183	353	209
	33	-2.0	28	53	35	13.8	120	263	159	-0.8	63	135	106	-3.3	130	258	140	-3.3	130	258	140
	34	-2.3	18	38	86	17.1	100	225	149	0.4	53	113	96	2.4	70	158	91	2.4	70	160	91
	35	-1.4	23	50	46	12.8	98	228	160	-0.9	60	128	109	-8.1	130	293	160	-8.1	128	293	160
	36	-2.1	18	38	37	11.5	105	235	152	-0.4	58	123	99	-5.9	73	178	104	-5.9	75	183	103
	38	-1.6	30	58	112	12.3	123	265	157	0.3	88	173	121	-1.0	135	265	153	-1.0	133	263	142
	39	-2.5	40	73	110	24.7	145	298	167	-0.5	65	143	118	1.5	140	273	162	1.5	133	263	147
	40	-2.0	23	43	90	0.7	103	230	150	-1.5	58	123	121	5.3	125	250	132	5.3	128	253	135
Block IIR	**41**	-0.6	15	28	31	-1.2	88	190	127	1.6	58	113	109	-1.5	33	70	113	-1.5	35	78	113
	43	0.5	15	28	32	-11.3	80	175	127	2.1	60	118	102	-0.7	35	83	101	-0.7	40	90	105
	44	0.4	15	28	37	-19.3	90	198	131	1.0	58	118	117	0.7	100	228	117	0.7	100	228	118
	45	-0.4	15	28	85	11.8	95	198	133	2.1	60	123	102	-2.0	28	60	69	-2.0	33	70	100
	46	-0.9	15	30	58	0.4	95	205	135	1.0	58	113	107	1.8	50	128	85	1.8	53	130	91
	47	0.0	15	28	26	15.3	90	195	129	0.9	60	125	91	11.0	65	178	109	11.0	68	178	108
	48	0.0	15	30	37	6.4	83	188	135	1.1	65	128	107	-2.3	38	85	74	-2.3	40	90	94
	50	-1.0	15	28	60	2.3	78	168	138	0.8	45	98	113	-0.9	25	55	62	-0.9	28	60	86
	51	-0.5	13	25	66	-11.9	88	190	122	1.6	60	118	94	-1.2	28	55	87	-1.2	30	63	94
	52	-0.2	15	28	51	5.0	93	200	123	0.7	55	113	74	-2.8	48	123	114	-2.8	50	125	112
	53	-0.7	15	28	26	11.2	103	225	148	0.8	68	148	117	0.5	53	148	97	0.5	55	150	102
	54	-0.9	15	30	87	19.2	88	188	127	2.0	58	113	106	-1.1	28	63	80	-1.1	30	70	84
	55	-1.0	15	30	30	6.6	90	193	132	0.9	53	108	95	-0.2	25	48	36	-0.2	28	58	44
	56	-1.4	15	28	36	9.9	85	185	125	-0.1	63	118	114	-3.2	25	50	51	-3.2	28	58	64
	57	-0.6	15	33	51	14.6	113	248	148	0.8	65	135	112	4.6	48	135	104	4.6	50	138	101
	58	-0.1	15	30	69	1.1	95	203	137	0.8	50	108	119	0.2	25	53	76	0.2	28	60	88
	59	-0.7	13	25	33	-5.3	83	180	128	0.6	63	123	118	-2.1	28	63	38	-2.1	33	70	89
	60	0.5	15	28	34	-1.3	83	173	121	1.1	50	103	104	1.3	25	50	87	1.3	28	60	85
	61	-0.8	13	25	31	8.6	78	170	122	1.8	55	108	105	-0.7	28	58	103	-0.7	30	68	114
Block IIF	**62**	-0.3	18	35	43	-2.9	80	170	140	1.5	48	98	121	-3.0	20	43	62	-3.0	30	60	82
	63	0.5	15	33	35	-36.5	93	203	137	1.4	63	128	115	-4.4	23	53	76	-4.4	33	70	82
	64	-1.7	20	38	39	19.6	70	153	152	1.6	50	98	104	-3.0	28	68	94	-3.0	38	85	93
	65	0.2	25	45	27	-13.6	98	208	135	-1.7	55	115	108	0.4	108	230	119	0.4	110	235	121
	66	0.1	18	38	41	-5.7	95	215	158	1.8	45	100	133	-0.4	23	48	65	-0.4	33	70	104
	67	3.0	20	50	42	-39.5	95	218	153	4.3	63	115	86	-1.0	25	53	30	-1.0	38	88	56
	68	-1.7	30	58	42	7.4	103	248	168	-8.9	50	118	129	-16.5	38	78	50	-16.5	50	105	85
	69	20.0	28	45	34	-162	208	455	256	9.9	105	250	141	-2.4	18	40	24	-2.4	40	108	70
	IIA	-2.0	25	63	102	13.2	118	273	165	-0.7	63	143	117	-0.1	105	248	134	-0.1	103	240	129
	IIR	-0.4	15	28	56	3.3	90	195	133	1.1	58	118	111	0.1	35	103	104	0.1	38	108	104
	IIF	0.1	20	38	39	-14.4	88	195	146	0.9	53	113	121	-2.7	28	120	94	-2.7	38	128	97
	All	-0.9	18	43	81	5.3	98	223	149	0.5	60	125	114	-0.1	50	185	122	-0.1	53	180	119

Table 1. *Radial, Along-Track, Cross-Track, Clock, and IURE Errors for all satellites. For each error the mean value, 68% bound, 95% bound, and overbounding sigma value are listed. All values are in centimeters.*